Chemistry Group Report No. 182, 1967 (unpublished) and references cited therein.

[6] Note that the apparent i-dependent terms in $H^{\gamma}(\gamma=a, \beta)$ [Δ_1 and Δ_2 of Eqs. (15a), (15b) of I] can be shown to be identically zero, using the definition of $\Lambda^{s}_{\gamma,t}$ [see Eq. (3) above].

PHYSICAL REVIEW A VOLUME 3, NUMBER 3 MARCH 1971

X Radiation from Optical and Inner-Shell Transitions in a Highly Ionized Dense Plasma*

T. N. Lie†
Catholic University of America, Washington, D. C. 20017

and

R. C. Elton
Naval Research Laboratory, Washington, D. C. 20390

(Received 23 October 1970)

X-ray line emission originating from "optical" (dipole and intercombination) transitions in heliumlike copper, iron, and titanium and hydrogenic iron and titanium ions has been observed in a concentrated dense plasma formed in a linear low-pressure discharge. In addition, emission from inner-shell x-ray transitions in Fe XIX-XXIV and Ti XV-XX ions has been identified. The measured wavelengths are compared with theoretical predictions and other observations. Continuum emission at wavelengths shorter than the Lyman-series limit for hydrogenic species has been used for electron temperature and density determination and as evidence supporting a thermal-electron collisional ionization model. Plasma dynamics studies indicate the existence of an axially propagating radial pinch, collapsing near the anode to a minute point.

I. INTRODUCTION

Solar-flare observations[1,2] from rockets and orbiting satellites have led to a tentative identification[2] of certain x-ray spectral lines arising from optical transitons in hydrogenic and heliumlike ions of heavy metallic elements, and from blended inner-shell transitions. Such features in these elements were not observed previously in laboratory plasmas. Recently, Cohen *et al.*,[3] using a high-energy vacuum spark source, obtained laboratory x-ray spectra of somewhat lower resolution which indicated the emission of resonance lines from similar optical transitions in ions of electrode material. Meanwhile, calculations of $K\alpha$ inner-shell transitions for all stages of ionization[4] and in more detail for lithiumlike ions[5] have been carried out. No laboratory or solar-flare data with adequate resolution for meaningful comparison with the calculations have been reported for inner-shell transitions in heavy metallic ions.

In this paper, we describe the obtainment and identification (with improved resolution) of such x-ray spectra including inner-shell transitions in multiply ionized copper, iron, and titanium. The laboratory source used was a highly concentrated point plasma produced in a low-pressure discharge (or vacuum spark). The results of the spectral analysis are compared with the existing predictions.

It is equally interesting to learn as much as possible concerning the detailed state of the plasma from which the x-radiation originates, and how it is formed. Towards this end, a number of phenomenological studies[6-8] have been made previously on various vacuum spark sources in order to relate the x-ray emission and the discharge characteristics. However, conclusions drawn from these studies are, in general, insufficient to account for the observation of concentrated x-ray emission arising from highly ionized atoms of heavy elements. In this paper, the electron temperature and density at the time of peak x-ray emission in the concentrated plasma region have been estimated, and the time-dependent behavior of the discharge plasma column has been studied using an image-converter camera. The results obtained are related to the time-resolved spectroscopic signals.

II. EXPERIMENTAL ARRANGEMENT

A. Plasma Source

A schematic diagram of this device is shown in Fig. 1. A cathode 2.5 cm in diam separated by 0.6 cm from a smaller anode of 0.4-0.7 cm diam was originally used, with a metallic cylinder acting as a current return from the cathode to a capacitor. However, the metallic cylinder was later replaced by a 5-cm-diam Pyrex tube and the current return straps were placed outside the glass cylinder. This arrangement was more convenient for observations and even improved the over-all

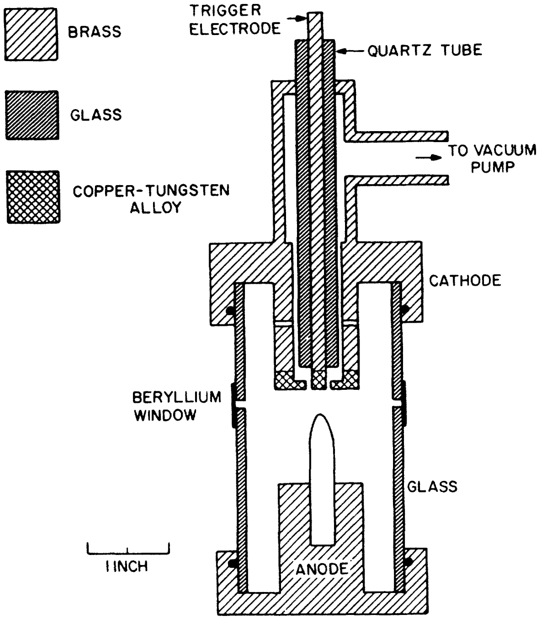

FIG. 1. Schematic diagram of the apparatus.

performance of the source. The anode was later modified to include a pointed tip which also improved the reproducibility, particularly in lateral position. The cathode and the trigger electrode are made of a low-erosion copper-tungsten (32-68% by weight, respectively) alloy.[9] Copper, iron, and titanium have been used as anode materials.

The positive electrode (anode) is connected directly to a 15-μF capacitor normally charged to +14 kV. Initiation of the discharge is performed by the trigger electrode inserted through the center of the cathode and connected through an air-gap switch to a 0.01-μF capacitor charged to +18 kV. The chamber is evacuated to a pressure of $\sim 10^{-5}$ Torr and the spark is initiated at this pressure. A maximum current of 100 kA is reached in 1.8 μsec.

This device produces a plasma concentrated at a point (or points) close (1–2 mm) to the anode tip from which the most intense x-ray flux originates, as evidenced from pinhole x-ray photographs taken through a 0.075-mm-thick beryllium window. The size of the point plasma is smaller than the available pinhole diameter (0.25 mm), and a closer examination using point-projection x-ray photography[10] of a fine mesh screen of a heavy element often showed a clear resolution with a grid up to 1500 lines/in. This indicates that a radiating dense plasma is obtainable with a cross section of diameter as small as 0.015 mm.

B. Spectrometer

X radiation emitted from the point-plasma source and transmitted through a 0.075-mm-thick beryllium foil has been analyzed using a simple flat crystal of lithium fluoride in the first spectral order. X radiation from the point source covers the crystal surface and subtends a varying incident Bragg angle across the crystal surface. The resolution obtained with such a simple (but sensitive) spectrometer is dependent on the size of the x-ray source (0.015 mm in this case), but even more on the shot-to-shot reproducibility of the lateral location of the plasma, since, for a typical film exposure, as many as 50–200 discharges are required. This reproducibility in lateral position was improved to be better than ± 0.3 mm by using a pointed-tip anode.

Although the x radiation of interest originates mainly from the point plasma, some interference occurred from the intense characteristic radiation from the entire anode surface, and from some portions of the electrode gap. Further improvement in the spectral clarity was obtained with spatially resolved (axially) spectra. These were obtained by placing a narrow (0.5-mm) slit of lead on the x-ray window and oriented perpendicular to the discharge axis. This space resolution showed that the spectral lines arising from atoms in higher stages of ionization originate entirely from a location a few millimeters above the anode tip (presumably from the concentrated dense plasma), whereas the $K\alpha$ and $K\beta$ lines characteristic of the element are emitted predominantly at the anode surface.

III. RESULTS

A. Time-Integrated Spectra

Microdensitometer scans of the time integrated spectra for copper, iron, and titanium anode materials were obtained and are shown in Figs. 2(a) and 2(b) for the latter two, respectively. Characteristic lines of $K\alpha$ and $K\beta$ (emitted from the anode tip) in the space-resolved spectra were used as standards for the absolute wavelength measurement. These standards were obtained from the anode-tip region since the "normal" characteristic $K\alpha$ line in the concentrated plasma region is weak and masked by a blend of nearby $K\alpha$ lines from ions in low stages of ionization.

A doublet feature between $K\alpha$ and $K\beta$ common to these three cases is associated with heliumlike optical ($1s^2$-$1s2p$) and lithiumlike inner-shell $1s^2nl$-$1snl2p$) transitions. The observation of such inner-shell "satellite" lines comparable in intensity to the adjacent heliumlike resonance line is consistent with an increasing trend towards higher nuclear charge along the isoelectronic sequence, as reported earlier for ions of carbon,[11,12] oxygen,[13] magnesium,[14] neon,[15,16] and argon.[15] In the high-density laboratory experiments, the upper levels for these transitions are populated mostly by electron collisional inner-shell excitation in the lithiumlike

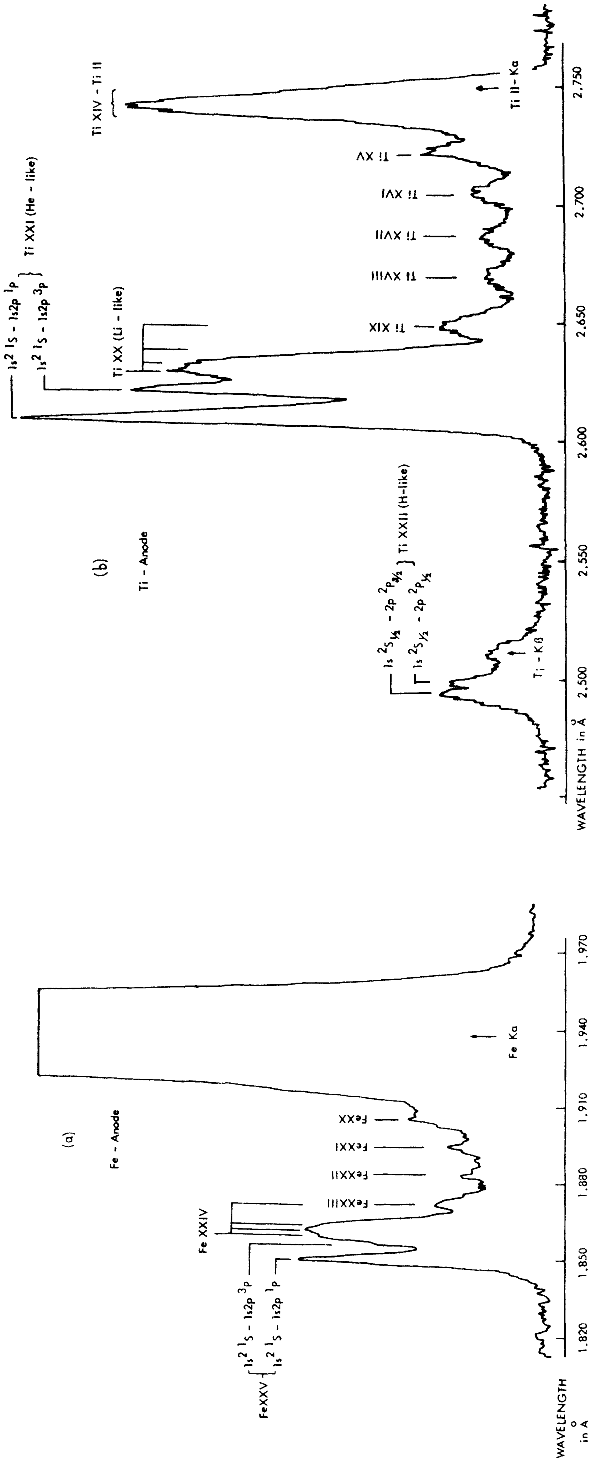

FIG. 2. Microdensitometer scans of x-ray emission spectra obtained with an iron (a) and a titanium (b) anode tip. The iron spectrum (a) is emitted from the entire electrode gap; the titanium spectrum (b) is space resolved and scanned at the concentrated plasma location.

species, and possibly collisional inner-shell ionization of berylliumlike ions.[5] Also, a generally broadened *Kα* feature is believed to be a blend of inner-shell transitions in particularly low stages of ionization where the wavelength intervals are small[4] (see Fig. 3).

In the spectrum of iron, a series of relatively strong resolved spectral lines are associated with optical transitions in heliumlike Fe xxv of the type $1s^2\,{}^1S$-$1snp\,{}^1P$ for $n = 2, 3, 4$ [see Fig. 2(a) for $n = 2$ and Table I for measured wavelengths]. Also in Fig. 2(a), the positions of the $1s^2\,{}^1S$-$1s2p\,{}^3P$ intercombination line of Fe xxv and the more intense of the (as many as five) inner-shell transition lines[5] in lithiumlike Fe xxiv of (mainly) the type $1s^2 2l$-$1s2l2p$ are indicated. Also listed in Table I is the measured wavelength for the $1s^2\,2l$-$1s2l3p$ inner-shell line in Fe xxiv.

There are a number of weaker lines lying between the lithiumlike Fe xxiv line and the blended normal characteristic *Kα* line which are identified as inner-shell *Kα* transitions of intermediate stages of ionization, i.e., emitted from Fe xix through Fe xxiii, which are not blended with the broad feature emitted mainly from the lowest ion stages. [The Fe xix inner-shell line is not resolved in the spectrum in Fig. 2(a) as it was in others obtained.]

The measured displacement of these inner-shell lines from the singlet resonance line of the heliumlike species is compared with Hartree-Fock calculations by House.[4] The good agreement between the two is indicated in Fig. 3, where it is seen that the wavelength intervals between adjacent stages of ionization remain small proceeding from Fe ii (i.e., normal Fe -*Kα*) through Fe xviii, but change to larger values beginning with Fe xix. This change is the result of the removal of $n = 2$ shielding electrons. The absolute wavelengths for the inner-shell lines in titanium and iron are listed in Table I. These agree within the estimated accuracy of the measurement with values given by House which were adjusted slightly for each element to fit with experimental and extrapolated data for low and high degrees of ionization. For one case, namely Ti xix, Cowan[17] obtained a result similar to that of House and was further able to account for the necessary adjustment mostly by a relativistic correction, which results in the second value given in Table I. The possibility that these inner-shell lines contain contributions from *Kα*-type transitions in lower-stage ions with additional vacancies (to the 1*s*) in the $n = 2$ shell is considered to be small, since the simultaneous removal of both $n = 2$ electrons and a 1*s* electron is improbable with the rapid filling of such vacancies from higher levels. The observation of heliumlike ions with no $n = 2$ shielding electrons is further evidence for sequential valence-electron removal.

TABLE I. Comparison between presently measured wavelengths and existing data.

Ion	Transition	Measured wavelength (Å) (±0.005 Å)	Previous results Experiment (Å)	Theory (Å)	Ref.
Ti XV	$K\alpha$ Inner-shell	2.721		2.720	4
Ti XVI	$K\alpha$ Inner-shell	2.704		2.704	4
Ti XVII	$K\alpha$ Inner-shell	2.686		2.687	4
Ti XVIII	$K\alpha$ Inner-shell	2.667		2.669	4
Ti XIX	$K\alpha$ Inner-shell	2.648		2.651 2.649	4 17
Ti XX	$1s^2 2s\ ^2S - 1s2s2p\ ^2P$	2.631		2.635	4
Ti XXI	$1s^2\ ^1S_0 - 1s2p\ ^1P_0$	2.612	2.62	2.619	3, 4
	$1s^2\ ^1S_0 - 1s2p\ ^3P_1$	2.623		2.622	5[a]
Ti XXII	$1s\ ^2S_{1/2} - 2p\ ^2P_{1/2}$	2.501			
	$1s\ ^2S_{1/2} - 2p\ ^2P_{3/2}$	2.496			
Fe XIX	$K\alpha$ Inner-shell	1.918		1.917	4
Fe XX	$K\alpha$ Inner-shell	1.906		1.907	4
Fe XXI	$K\alpha$ Inner-shell	1.896		1.897	4
Fe XXII	$K\alpha$ Inner-shell	1.886		1.886	4
Fe XXIII	$K\alpha$ Inner-shell	1.872		1.875	4
Fe XXIV	$1s^2 2s\ ^2S - 1s2s2p\ ^2P$	1.861	1.860	1.865	2, 4
	$1s^2 2s\ ^2S - 1s2s3p\ ^2P$	1.602			
Fe XXV	$1s^2\ ^1S_0 - 1s2p\ ^1P_0$	1.851	1.850	1.865	2, 4
	$1s^2\ ^1S_0 - 1s2p\ ^3P_1$	1.856	1.855	1.855	2, 5[a]
	$1s^2\ ^1S - 1s3p\ ^1P$	1.592	1.59		3
	$1s^2\ ^1S - 1s4p\ ^1P$	1.518			
Fe XXVI	$1s\ ^2S_{1/2} - 2p\ ^2P_{1/2}$	1.779			
	$1s\ ^2S_{1/2} - 2p\ ^2P_{3/2}$				
Cu XXVII	$1s^2 2s\ ^2S - 1s2s2p\ ^2P$	1.492		1.489	4
Cu XXVIII	$1s^2\ ^1S_0 - 1s2p\ ^1P_0$	1.484		1.481	4

[a] Values obtained from an extrapolation of the curve given in Ref. 5 and using the wavelength of the $1s^2\ ^1S_0 - 1s2p\ ^1P_0$ line from the present work.

It is interesting to note that the observed blend of Fe XXIV satellite lines is remarkably similar to that from a solar-flare spectrum obtained[2] recently. While the Fe XXIV $1s2s\ ^3S \rightarrow 1s^2\ ^1S$ magnetic dipole intercombination solar line will not contribute[18] at the high electron density in the laboratory plasma, the $1s^2 2p\ ^2P^0$-$1s2p^2\ ^2P^e$ inner-shell line of Fe XXIV (which is absent in the solar spectrum since the upper level cannot be populated by dielectric recombination[5]) may provide a compensating contribution in the laboratory plasma.

Finally, Fig. 2(b) shows a microdensitometer scan of a space-resolved x-ray spectrum taken at the concentrated plasma location using a titanium anode. In this case, the $1s^2\ ^1S$-$1s2p\ ^3P$ intercombination line of heliumlike Ti XXI is clearly resolved, and the corresponding $1s^2\ ^1S$-$1s2p\ ^1P$ resonance line is much more intense than the lithiumlike Ti XX inner-shell $K\alpha$ feature, for the somewhat lower nuclear charge (as discussed above). The wavelength intervals of $K\alpha$–inner-shell transitions for Ti XV–Ti XX ions are also plotted in Fig. 3. Again, a good agreement with the theory is obtained. Absolute wavelengths are listed in Table I.

Another interesting feature in the spectrum obtained with the titanium anode is a "doublet" located at the shorter-wavelength side of the $K\beta$ line. This radiation originates in the point plasma as confirmed

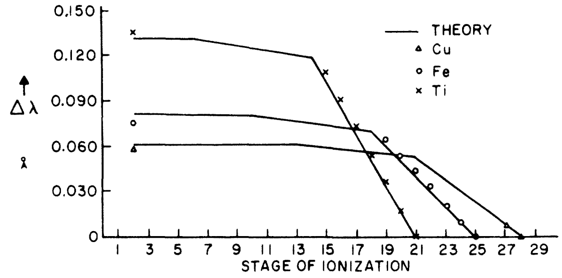

FIG. 3. A comparison between experimental and theoretical (see Ref. 4) results for the displacement Δλ (in Å) of the resolved inner-shell transition lines from the resonance line of the heliumlike ion. The stage of ionization 2 refers to the singly ionized atom, for which the measured points correspond to normal characteristic $K\alpha$ transitions.

by the space-resolved spectrum. These two lines (separated by ~ 0.005 Å) are associated with optical Lyman-α transitions $1s\ ^2S_{1/2}$-$2p\ ^2P_{1/2}$ and $1s\ ^2S_{1/2}$-$2p\ ^2P_{3/2}$ in hydrogenlike Ti XXII. Absence and considerable weakness of hydrogenic lines in time-integrated spectra of copper and iron, respectively, are believed to be due to a marginal total plasma confinement time compared to the ionization relaxation time.[15]

B. Time-Resolved X-Ray Spectra and Kinetics of Discharge

The discharge takes place at an ambient pressure of ~ 10^{-5} Torr, with probably some additional gaseous particles occluded from the electrodes when the trigger spark is initiated. There is no evidence that the discharge begins along an insulating surface, and therefore it is considered to be confined mainly to the electrode gap during the time of interest. A time-dependent study of both the x-ray spectrum and the luminous discharge plasma behavior within the electrode gap was made in order to understand better the physical processes involved in this source.

Figure 4 illustrates oscillographic traces showing the time correlation between *dI/dt* and x-ray spectroscopic signals from a scintillation detector behind a (lead) slit in the film plane. All of these signals are normalized (in time) to the *dI/dt* waveform. One notices here that x-ray emission takes place during the first quarter cycle of the discharge and that each x-ray pulse signal is approximately coincident with significant *dI/dt* dips, which is a typical discharge characteristic observed in linear pinch and coaxial gun plasma focus devices. Figure 5(a) shows the axial motion of the plasma as obtained from streak photography through a slit oriented parallel to the discharge axis. Radial motion is also studied at various axial positions of the electrode gap [see Fig. 5(b)].

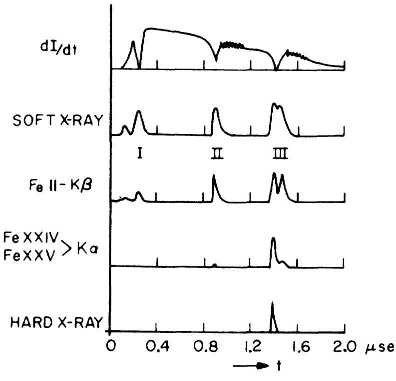

FIG. 4. Oscillograms showing the *dI/dt* waveform and the x-ray spectral signals from the scintillation detector. The indicated phases (I, II, III) of the discharge are as discussed in the text and also included (II, III) in Fig. 5.

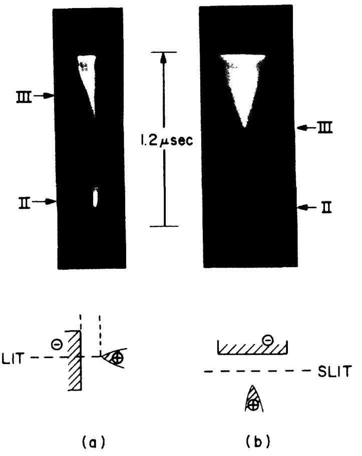

FIG. 5. Streak photographs showing axial (a) and radial (b) motions of the plasma column. Here the alignment of the viewing slit relative to the discharge axis is shown. In (b) the plasma is viewed 2 mm from the anode tip. The indicated phases (II, III) of the discharge are as discussed in the text and also included in Fig. 4.

The discharge event and the x-ray signals may be divided into three phases (I, II, III) as indicated in Figs. 4 and 5. Directional x-ray detection using a collimator and a scintillation detector reveals that the relatively slowly rising x-ray signal at the very beginning of the discharge and the following pulse (in phase I) are emitted, respectively, from the entire anode surface and from the very tip of the anode. The mechanism involved in anode x-ray emission during this phase of the discharge has been studied recently.[19] The x-rays emitted in phase II originate in a relatively large volume of plasma located somewhere in the anode half of the electrode gap. This is observed as a faint cloud in the pinhole x-ray photograph and consists of low-energy (soft) x-ray line emission arising from normal $K\alpha$ and $K\beta$ transitions and x-ray continuum (see Fig. 4). This x-ray burst coincides in time with the enhanced luminosity [Fig. 5(b)] emitted during a radial contraction. This contraction originates near the cathode at early times and propagates towards the anode region with a velocity of ~ 9 cm/μsec [see Fig. 5(a)].

Following the phase-II burst by about 0.5 μsec, a more luminous plasma front propagates towards the cathode at a velocity of ~ 6 cm/μsec. The main x-ray burst (phase III) – in which we are most interested – is emitted from the concentrated point plasma observed in pinhole photographs and coincides in time with the formation of this bright luminosity near the anode tip and with the sudden start of a radial expansion (velocity of ~ 2 cm/μsec) following a dark period [see Fig. 5(b)]. This x-ray burst represents the most intense x-ray emission of all the three phases. As can be seen in Fig. 4, the signal includes x radiation arising from the main optical and inner-shell ion features. High-energy continuum (bremsstrahlung and recombination) radiation is also pronounced during this phase as detected through absorbers of sufficient thickness to reject all line emission.

C. Electron Density and Temperature

In an effort to form a model for the rapid generation of the very high stages of ionization observed in the x-ray spectra, the electron density and temperature were estimated from the measured x-ray continuum emission at wavelengths shorter than the lower limit for line emission, i.e., the Lyman-series limit for hydrogenic ions.

The electron temperature at peak x-ray emission in the concentrated plasma region was deduced[20] by the x-ray absorption method for determining the continuum energy distribution characteristic of bremsstrahlung or radiative recombination (collisional recombination is negligible[21]) radiation. The relative continuum emission through a pair of absorbers was obtained by recording the photoelectric signal from plastic scintillation detectors. At higher temperatures, gold foil was used with thickness ranging from 250 to 750 mg cm^{-2}; for the lower temperatures, nickel with thickness ranging from 225 to 950 mg cm^{-2} was used. The electron kinetic temperatures thus measured varied from discharge-to-discharge over a range of $kT = 2-100$ keV.

An order-of-magnitude estimate of $\sim 10^{20}$ cm^{-3} for the electron density was obtained from the absolute continuum emission, with the uncertainty associated with the size of the radiating volume, inaccuracies in the absolute intensity determination, and an uncertainty in the magnitude of the pure bremsstrahlung emission at the longer wavelengths as compared to the predominantly recombination radiation measured beyond the series limit. The absolute continuum emission was obtained by extrapolating the emission measured through the aluminum absorber to all wavelengths, correcting for the aluminum transmission, recombination edge steps, and for the solid angle of view. Kodak No-Screen x-ray film was used for recording and the film calibration was taken from Dozier *et al.*[22]

Although these electron density measurements were obtained from continuum emission from high-Z metallic ions, a compression and ionization of only a fraction of the initial ambient-gas density ($\sim 3\times 10^{11}$ molecules/cm^3) could produce the measured electron density. In arriving at the above figure for the electron density, it was assumed that the radiating plasma consisted solely of hydrogenic and heliumlike ions and that the ordinary hydrogenic formulas[21] were applicable.[23] An uncertainty in the ratio of the metallic and ambient-gas contributions to the plasma density does not significantly alter the above magnitude estimate for the electron density.

IV. DISCUSSION

The rapid formation of a minute and highly concentrated plasma which emits x-ray line radiation arising from highly stripped ions of high-Z atoms immediately poses a question as to the processes involved. The most plausible model suggested by the data obtained here is ionization by thermal-electron collisions, rather than a nonthermal electron beam model which has been proposed[6,7,24] to explain high-energy x radiation from similar devices. Comparing the normal $K\beta$ line characteristic of titanium with the Ti XXI He-like or Ti XX Li-like ion lines in Fig. 2(b) (which is a microdensitometer scan at the concentrated plasma location), one notices the domination of the ionic lines over the normal characteristic lines. The shift of the feature near the normal characteristic $K\alpha$ line is also due to a dominance of ion emission. This adds support to the thermal-electron ionization model.

The measured electron temperature of $kT \approx 2-100$ keV at the concentrated plasma is high enough to provide electrons with sufficient energy to generate the ions and excited states for the observed emission, provided sufficient relaxation time for ionization is available. Assuming stepwise ionization, the total relaxation time for ionization to Fe XXV is estimated[21] to be of the order of 10^{-7} sec for the measured plasma parameters. Particle confinement times of this duration are justified by ion gyro-radii as short as a few microns for local magnetic fields estimated from the discharge current. Such limited confinement times are thought to explain the weak hydrogenic lines in the spectrum of iron.

The detailed mechanism involved in the formation of the intense concentrated plasma may be too complex and difficult to deduce with the data available at present. It seems most probable however that the radial constriction that forms early near the cathode and is observed to propagate towards the anode is driven by a longitudinal magnetic field gradient. It is further suggested in analogy to the coaxial gun plasma focus device – for which detailed numerical simulation has been carried out[25] – that the most severe constriction of the plasma column, resulting in the observed concentration, takes place near the anode tip around which a relatively cold dense plasma is formed while maintaining pressure balance in a region of rapid conductive cooling to the anode surface. A high magnetic field in this region could penetrate the low conductivity plasma near the anode tip and create a magnetic pressure which increases with decreasing radius, resulting in the high compression observed. This opposing magnetic pressure (due to a fountainlike current feature with a vortex at the anode tip) could produce the observed cathode-directed motion of the plasma.

ACKNOWLEDGMENT

The authors wish to thank Dr. D. F. Düchs for his helpful criticisms.

---

*Research supported in part by the National Aeronautics and Space Administration under Grant No. NGR-09-005-025.

†Present address: Naval Research Laboratory, Washington, D. C. 20390.

[1] G. Fritz, R. W. Kreplin, J. F. Meekins, A. E. Unzicker, and H. Friedman, Astrophys. J. 148, L133 (1967); see also J. F. Meekins, R. W. Kreplin, T. A. Chubb, and H. Friedman, Science 162, 891 (1968).

[2] W. M. Neupert and M. Swartz, Astrophys. J. Letters 160, L189 (1970); see also W. M. Neupert, W. Gates, M. Swartz, and R. Young, Astrophys. J. 149, L79 (1967).

[3] L. Cohen, U. Feldman, M. Swartz, and J. H. Underwood, J. Opt. Soc. Am. 58, 843 (1968).

[4] L. L. House, Astrophys. J., Suppl. 18, 21 (1969).

[5] A. H. Gabriel and C. Jordan, Nature 221, 947 (1969).

[6] S. V. Lebedev, S. L. Mandel'shtam, and G. M. Rodin, Zh. Eksperim. i Teor. Fiz. 37, 349 (1959) [Soviet Phys. JETP 37, 248 (1960)].

[7] S. K. Händel, Arkiv Fysik 28, 303 (1964); also S. K. Händel and J. M. Berg, *ibid.* 31, 1 (1965).

[8] L. N. Khudyakova, E. K. Gutnikova, and L. V. Tarasova, Zh. Tekhn. Fiz. 34, 2044 (1964) [Soviet Phys. Tech. Phys. 9, 1572 (1965)].

[9] "Elkinit-3," manufactured by P. R. Mallory Mettalurgical Co., Indianapolis, Ind.

[10] V. E. Cosslett and W. C. Nixon, *X-Ray Microscopy* (Cambridge U. P., London, 1960), Chap. 3.

[11] B. Edlén and F. Tyrén, Nature 143, 940 (1939).

[12] B. Edlén, Physica 13, 545 (1947).

[13] N. V. Roth and R. C. Elton, Naval Research Laboratory Report No. NRL-6638, 1968 (unpublished).

[14] H. Flemberg, Arkiv Math. Astron. Fysik 28A, 1 (1942); see also Ref. 12, p. 553.

[15] N. J. Peacock, R. J. Speer, and M. G. Hobby, J. Phys. B. 2, 798 (1969).

[16] G. A. Sawyer, J. Quant. Spectry. Radiative Transfer 2, 467 (1962).

[17] R. D. Cowan (private communication).

[18] H. R. Griem, Astrophys. J. 156, L103 (1969); 161, L155 (1970).

[19] H. M. Epstein, W. J. Gallagher, P. J. Mallozzi, and T. F. Stratton, Phys. Rev. A 2, 146 (1970).

[20] R. C. Elton, Naval Research Laboratory Report No. 6738, 1968 (unpublished).

[21] R. C. Elton, in *Methods of Experimental Physics-Plasma Physics*, edited by H. R. Griem and R. H. Lovberg (Academic, New York, 1970), Chap. 4.

[22] C. M. Dozier, J. V. Gilfrich, and L. S. Birks, Appl. Opt. 6, 2136 (1967).

[23] That this assumption is reasonable is seen from the large increase in ionization potential along the isoelectronic sequence between lithiumlike and heliumlike ions. Therefore, the heliumlike and hydrogenic ion populations will dominate when they exist. The strong dependence on effective charge $Z(Z^2$ for bremsstrahlung and Z^4 for radiative recombination) of the continuum radiation further favors these ions.

[24] S. V. Lebedev, Zh. Tekhn. Fiz. 38, 171 (1968) [Soviet Phys. Tech. Phys. 13, 119 (1968)].

[25] K. V. Roberts and D. E. Potter, *Methods in Computational Physics*, edited by B. Alder, S. Fernbach, and M. Rotenberg (Academic, New York, 1970).

PHYSICAL REVIEW A VOLUME 3, NUMBER 3 MARCH 1971

Muonium. II. Observation of the Muonium Hyperfine-Structure Interval*

J. M. Bailey,† W. E. Cleland,‡ V. W. Hughes, R. Prepost, § and K. Ziock‖
Gibbs Laboratory, Yale University, New Haven, Connecticut 06520

(Received 1 July 1970)

A full discussion is given of the microwave-spectroscopy resonance method of measuring the hyperfine-structure interval $\Delta\nu$ of the ground state of muonium, including the theoretical value for $\Delta\nu$, the transition frequencies, and the resonance line shape. A complete description is also given of our experimental method of measuring $\Delta\nu$ at strong magnetic field. The initial experimental results gave $\Delta\nu = 4461.3 \pm 2.0$ MHz, in good agreement with the theoretical value $\Delta\nu = 4463.282 \pm 0.062$ MHz. The first observations of muonium chemistry are described.

I. INTRODUCTION

The discovery[1,2] that muonium is formed when muons are stopped in argon gas and the rough measurement of its ground-state hyperfine-structure interval $\Delta\nu$ with the use of a static magnetic field[2,3] indicated that $\Delta\nu$ could be measured in a precision microwave resonance experiment. The principles of the experiment are to form polarized muonium by stopping polarized muons in a gas, to induce with microwave power a resonance transition between two unequally populated hfs magnetic substates which will result in a change in muon spin direction, and to observe this transition through

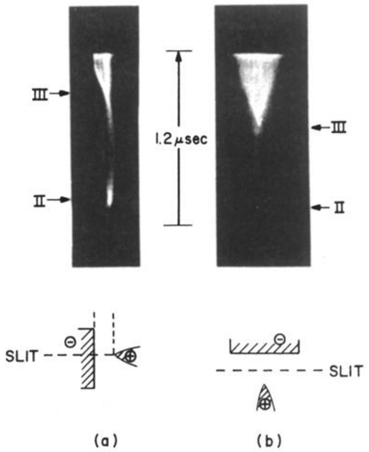

FIG. 5. Streak photographs showing axial (a) and radial (b) motions of the plasma column. Here the alignment of the viewing slit relative to the discharge axis is shown. In (b) the plasma is viewed 2 mm from the anode tip. The indicated phases (II, III) of the discharge are as discussed in the text and also included in Fig. 4.